Characterization of Uranium and Uranium-Zirconium Deposits Produced in Electrorefining of Spent Nuclear Fuel

by

T.C. Totemeier

Argonne National Laboratory-West
P.O. Box 2528
Idaho Falls, ID 83403-2528

Conference Paper to be submitted for presentation at the
30th IMS Annual Convention
Seattle, WA
July 20-23, 1997

Work supported by the U.S. Department of Energy, Reactor Systems, Development and Technology, under Contract W-31-109-Eng-38.

DISCLAIMER

Abstract

This paper describes the metallurgical characterization of deposits produced in molten salt electrorefining of uranium and uranium – 10 wt.% zirconium alloy. The techniques of characterization are described with emphasis on considerations given to the radioactive and pyrophoric nature of the samples. The morphologies observed and their implications for deposit performance are also presented—samples from pure uranium deposits were comprised of chains of uranium crystals with a characteristic rhomboidal shape, while morphologies of samples from deposits containing zirconium showed more polycrystalline features. Zirconium was found to be present as a second, zirconium metal phase at or very near the uranium-zirconium dendrite surfaces. Higher collection efficiencies and total deposit weights were observed for the uranium-zirconium deposits; this performance increase is likely a result of better mechanical properties exhibited by the uranium-zirconium dendrite morphology.

ARGONNE NATIONAL LABORATORY (ANL) is currently demonstrating an electrometallurgical process for treatment of spent nuclear fuel (SNF). Due to the cancellation of the Integral Fast Reactor (IFR) program for which it was developed, the electrometallurgical process has been redirected towards treatment of spent fuels from the Experimental Breeder Reactor – II (EBR-II) (1) and potentially other SNF owned by the U.S. Department of Energy (DOE) (2).

The key element of the treatment process is the electrorefining step. In the electrorefining step, chopped metallic spent fuel slugs contained in steel baskets are placed in a molten eutectic LiCl-KCl electrolyte bath and anodically dissolved. The cathode of the electrochemical cell is a bare steel mandrel which collects purified uranium. The fission product and actinide contaminants in the spent fuel typically either form chlorides and dissolve into the salt phase or remain as metals, ideally with the cladding hulls in the anode baskets. The fission products and actinides are incorporated into two waste forms—a stainless-steel based metallic form and a glass-bonded zeolite ceramic form (3).

The initial development of SNF electrorefining as it pertains to treatment of EBR-II fuel was carried out at the Argonne-East (ANL-E) site near Chicago, Illinois. The electrorefining technology has now been transferred to the Argonne-West (ANL-W) site near Idaho Falls, Idaho for a pilot-scale demonstration in the Fuel Conditioning Facility (FCF) hot cells using actual SNF from the EBR-II reactor (4). As part of the initial start-up activities for the FCF electrorefiner, 31 deposition runs have been made using either pure depleted uranium or an alloy of uranium and 10 wt.% zirconium (U-10Zr) as feed material.

Detailed metallurgical examinations were carried out on samples of the uranium deposits from several of the runs to determine the effects of operating parameters on the resulting macro- and micro-morphology of the uranium cathode deposit. These parameters included electrorefining mode, current density, mixing in the salt phase, and presence of zirconium in the feed material. This paper presents the techniques used to examine the radioactive and potentially pyrophoric deposit material, the results of the examinations, and the implications of the observed morphologies for the performance of the deposit in terms of total deposit weight and collection efficiency.

Experimental Procedures

Electrodeposition Conditions. The FCF electrorefiner is a 99 cm deep, 102 cm diameter cylindrical steel vessel with an operating temperature of 773 K located in the FCF purified Ar hot cell. The electrolyte is a molten LiCl-KCl eutectic (41 mol.% KCl) with nominally 1.6 mol.% UCl_3 dissolved in it; the electrolyte rests on a pool of molten cadmium whose height is approximately 10 cm from the vessel bottom. Four circular ports 25 cm in diameter are used to insert the anodes and cathodes into the electrolyte. Electrorefiner feedstock consisted of either pure U or U-10Zr alloy as pin pieces or chopped segments. The feedstock was loaded into perforated, rectangular baskets which served as anodes. A solid steel rod was inserted for use as a cathode.

Deposits were produced with a direct current power supply operating under controlled current conditions. Two modes of transport were used: direct transport, which used the filled basket assembly as an anode and the steel rod as a cathode; and deposition from the Cd pool, which used the U-

containing Cd pool as an anode. Uranium which is lost from the cathode during electrodeposition falls and dissolves into the Cd pool.

The process variables available in the preparation of the deposits included current magnitude, cell voltage, electrorefining mode, mixing in the salt and Cd phases, and U mass available for transport. As described below, it was found that the most important variable in determining the deposit morphology—and in turn deposit performance—was the presence of zirconium in the feed material. As such, the specific deposition conditions for each deposit described will not be presented in this paper. All deposits were prepared with cell voltages ranging from 0.77 V to 1.28 V, at currents as high as 300 A. Typically at least 10 kg of U was available for deposition; the weights of resulting deposits varied from 2.9 kg to 10.8 kg.

Sampling and Examination Procedures. Because the electrorefiner was designed for use with highly radioactive SNF, it is located in a shielded hot cell and all operations must occur remotely using manipulators. The samples described in this paper were not produced using actual SNF, so the radiation levels of the samples were low. However, the techniques described have been subsequently used with much more radiactive material, up to 8 R/hr total radiation field (mostly beta) for a sample weighing approximately 3 grams.

Small samples suitable for examination were removed from deposits in the FCF hot cell using manipulators. Clumps of material weighing between one and five grams were broken from representative areas at different locations of the deposit. Samples were removed from the following locations, as shown schematically in Fig. 1: top inside, top outside, middle outside, and bottom inside. The specific sampling locations for each deposit discussed are presented in Table 1. Note that all of the sample locations are on the periphery of the deposit. The restrictions of hot cell operations did not permit sampling from the interior of the deposit.

The samples were then placed into transfer tubes (Swagelok®-sealed stainless steel) and removed from the hot cell for examination and analysis. As part of preparation for examination, the deposit samples had to be exposed to an air environment, as opposed to the Ar environment of the hot cell. Because of the fine dendritic structure of the deposited material, its specific surface area is high. In order to mitigate any potential pyrophoric hazards associated with U in such a form the transfer tubes containing the samples were carefully opened in a fume hood under flowing Ar gas. The Ar gas flow was slowly reduced until only air remained. No visible signs of heating or oxidation were seen. Once the samples had been introduced in the air atmosphere, the residual salt adhering to the U metal was removed. Salt removal was accomplished by ultrasonic cleaning in an ethanol bath punctuated by small additions of distilled water.

Characterization of the cleaned samples was performed using standard metallographic and scanning electron microscopy (SEM) techniques. The precautions taken due to the radioactive nature of the samples were those routinely used for contamination control. Metallographic cross-sections of the samples were prepared by mounting an entire piece in either a cold epoxy resin or hot bakelite mount and then grinding the specimen until a suitable section was visible. Both unmounted samples and cross-sections were examined in a ISI SS40 SEM after Pd coating to minimize charging. Semi-quantitative energy-dispersive X-ray analysis (EDS) was performed in the SEM using a Kevex Micro-X 7000 system. In addition, the elemental compositions of the samples were determined by the ANL-W analytical chemistry laboratory using standard chemical techniques.

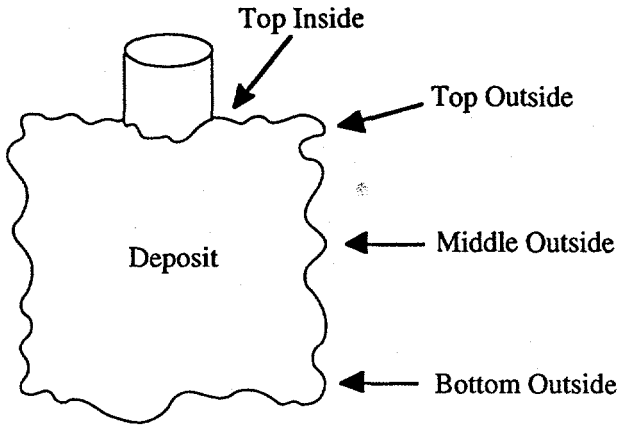

Fig. 1: Deposit sampling locations.

Observed Deposit Morphologies

Deposits Produced Using Pure U Feedstock. Deposits 3 and 8 were prepared using pure U as feed material. Table 1 gives the observed characteristics of the samples from these deposits in terms of morphology, crystal size, and presence of interior structure (described below). The macroscopic morphologies of these three deposits were similar—all showed long dendritic-shaped chains of U crystals. These chains appeared to slump under their own weight. It was clear from examination of the deposits through the hot cell window that a fairly broad range of crystal sizes were present on each individual deposit. It was not feasible, however, to obtain a proper distribution of crystals sizes and aspect ratios necessary to fully quantify differences between deposits. Hence the descriptions given below are only qualitative. At such a level of assessment, the observed morphologies were essentially identical. Fig. 2 is photograph of Deposit 3 taken through the hot cell window. The slumping of the deposit is readily evident. The deposit had a shiny metal color, which correlated with a relatively low residual salt content on the deposit surface. The crystals of Deposit 8 were also fairly large, similar to those from Deposit 3.

The shapes and arrangements of the U crystals constituting the dendritic chains were revealed by SEM examination. Fig. 3 shows an overview of a sample from Deposit 3. The dendrite-shaped chains of U were comprised of plate-like rhomboidal crystals linked end-to-end. The individual crystals varied in size, both within a single chain and from sample to sample. Fig. 3 shows a chain with relatively large crystals (sizes ranging from approximately 0.3 mm to 3 mm). X-ray diffraction of similar crystals by previous researchers has shown the growth direction to be (310) (5). Close examination of the crystal surfaces showed them to be essentially featureless. Only a fine oxide-like roughness was visible.

Table 1: Characteristics of Deposits Samples Examined.

Sample	Morphology: Crystal Size	Overall Zr Concentration	Surface Zr Concentration	Interior Structure	Zr Phases in Cross-Section
Cathode 3					
Top Outside	Long Chain of Large Rhombic Crystals: 0.3-3 mm	Not Applicable	Not Applicable	Yes	Not Applicable
Cathode 8					
Top Outside	Chain of Large Rhombic Crystals: 0.3-3 mm	Not Applicable	Not Applicable	Yes	Not Applicable
Middle Outside	Chains and Clumps of Larger Crystals: 20 μm - 2 mm	Not Applicable	Not Applicable	Yes	Not Applicable
Cathode 28					
Top Outside	Short Chain of Large Rhombic Crystals: 4 mm	3.5 wt.%	100 wt.%	Yes	Continuous: 3-10 μm Thick
Middle Outside	Large Polycrystalline Dendrite	11.5 wt.%	100 wt.%	No	Continuous: 5-20 μm Thick
Bottom Outside	Polycrystalline Dendrite	7.3 wt.%	29-58 wt.%	No	Many: 7-20 μm Thick
Cathode 30					
Top Inside	Agglomeration of Fine Grains: 150-300 μm	2.1 wt.%	79-90 wt.%	No	Many: 2-5 μm Thick
Top Outside	Agglomeration of Fine Grains: 300-700 μm	0.13 wt.%	15-37 wt.%	No	Few: 0.5 μm Thick
Cathode 31					
Top Inside	Aggregate of Blocky Crystals: 0.6-1.6 mm	465 ppm	20-67 wt.%	No	None
Top Outside	Large Branching Polycrystalline Dendrite	0.22 wt.%	6-24 wt.%	Not Available	Not Available
Middle Outside	Large Branching Polycrystalline Dendrite	0.13 wt.%	Not Available	No	None
Bottom Outside	Tangle of Fine Rhomboidal Crystals	0.46 wt.%	10-66 wt.%	Yes	Many: 2-5 μm Thick

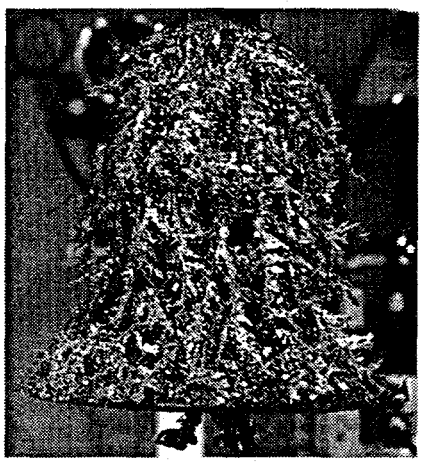

Fig. 2: Deposit 3. Maximum deposit diameter is 25 cm.

In sharp contrast to their exterior perfection, the interior structure of the crystals was highly complex, as revealed in metallographic cross-sections. Fig. 4 shows a cross-section of a large crystal sampled from Deposit 8. It was expected from the exterior views that the cross-sections would show homogeneous, solid, single crystal material; however, this was not the case. While no grain boundaries were observed in the crystal, the structure was neither homogeneous nor solid. Instead, the entire crystal was filled with a fairly fine and sometimes oriented structure. Similar structures were observed in all of the larger crystals examined. The structure usually took the form of interior platelets of U oriented along the long axis of the exterior crystal shape, as is seen at the right-hand side of Fig. 4. It was assumed that the gaps between the U platelets were filled with entrained salt prior to cross-section preparation. The gaps were not filled with mounting material, and any salt which was present would have been removed by the grinding and polishing procedures. There is no conceivable mechanism for the gaps to be true void space.

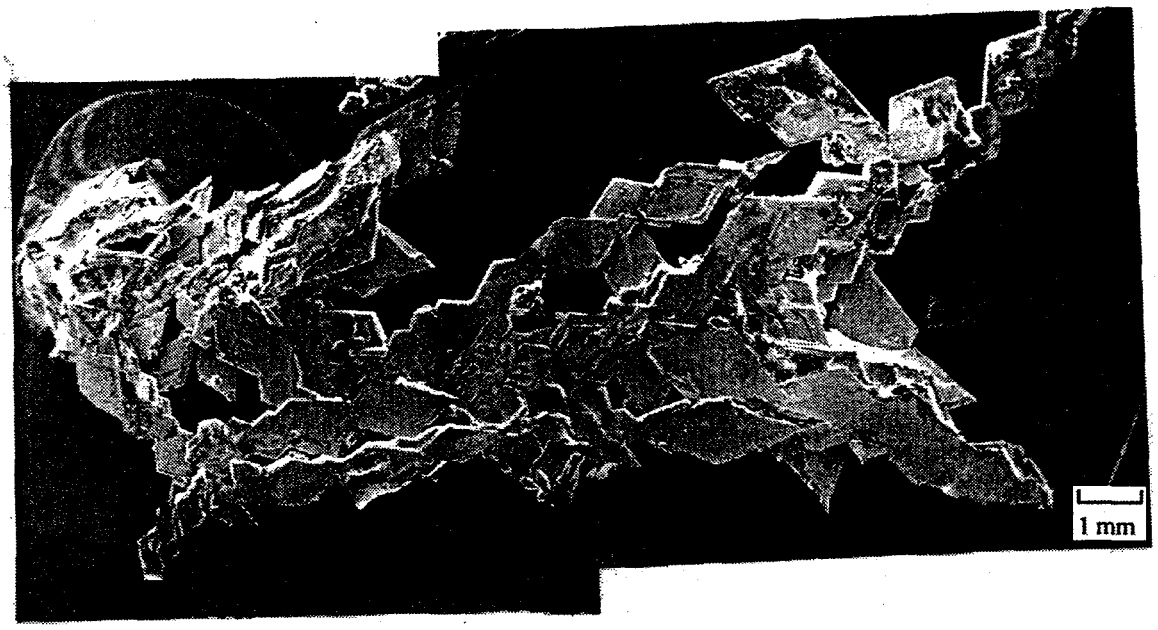

Fig. 3: Overview of a sample from Deposit 3 showing chains of linked rhomboidal uranium crystals (10X).

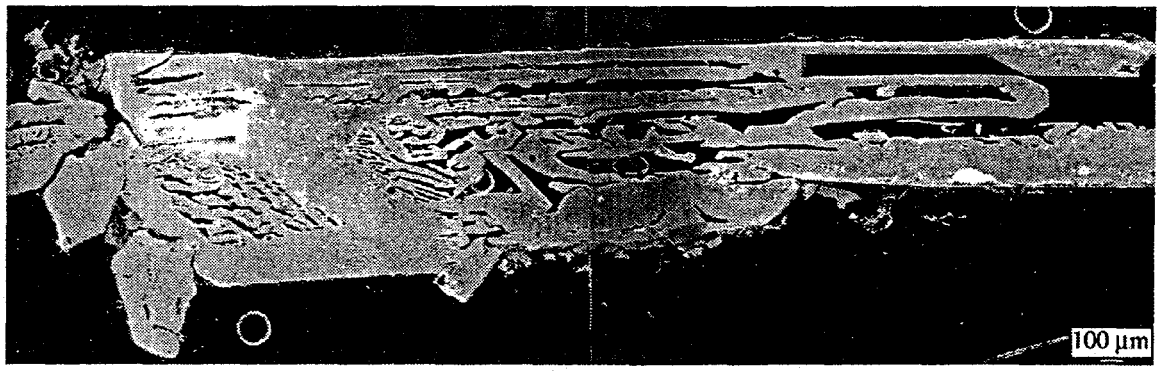

Fig. 4: Cross-section of a large crystal from a Deposit 8 sample showing complex internal structure (40X).

Although from the exterior nearly all U crystals appeared to be solid and single grained, a crystal was observed in a Deposit 8 sample with features suggesting a sequence for interior structure formation. This crystal is shown in Fig. 5. The faces of the crystal are very regular, with the exception of the one facing the viewer. This face is composed of fine platelets oriented parallel to the top and bottom (as seen in the figure) faces of the crystal. The platelets have a fairly regular spacing. The edges of the face appear to be "growing over" the platelets to form a smooth exterior surface. Hence a possible growth sequence suggests itself. The original growth is one of several platelets growing parallel to one another from a surface. At some point, the outside platelets change direction and grow over the middle plates, enclosing them in a seemingly perfect crystal. In this process the electrolyte salt is entrained in the crystal.

Deposits Produced Using U-10Zr Feedstock. Deposits 28, 30, and 31 were prepared using U-10Zr alloy as feed material. This alloy constitutes the majority of the EBR-II driver fuel to be treated in the demonstration project. Actual SNF, of course, also contains numerous fission product contaminants, but no attempts were made to simulate their presence. Previous electrorefining experience with U-Zr alloys in the laboratory-scale electrorefiner at ANL-E suggested that a different deposit morphology would be observed for U-Zr feedstock compared to pure U. Due to the similarity in redox potentials for U and Zr, under normal operating conditions (a cell voltage of approximately 0.7 V) some Zr deposits at the cathode along with U. A true separation of U and Zr is possible using lower cell voltages (less than approximately 0.4 V) (6).

Table 1 presents the observed characteristics of the U-Zr samples in terms of morphology, crystal size, surface Zr concentration, presence of interior structure, and presence of Zr phases. The macroscopic morphologies observed for these deposits were similar, and very different from the morphologies observed for the previous deposits which contained little or no Zr. A typical macroscopic morphology for Zr-containing deposits is shown in Fig. 6 for Deposit 30.

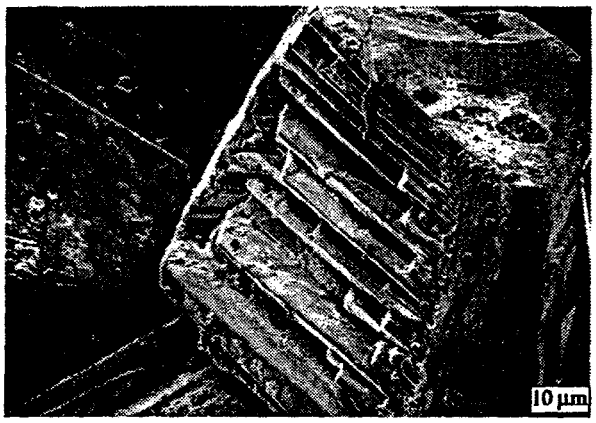

Fig. 5: Incomplete crystal in Deposit 8 sample (170X).

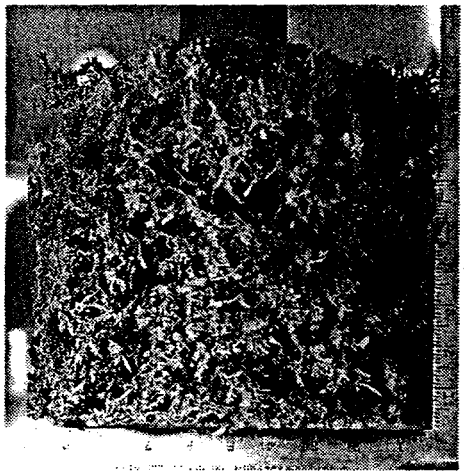

Fig. 6: Deposit 30. Maximum diameter is 25 cm.

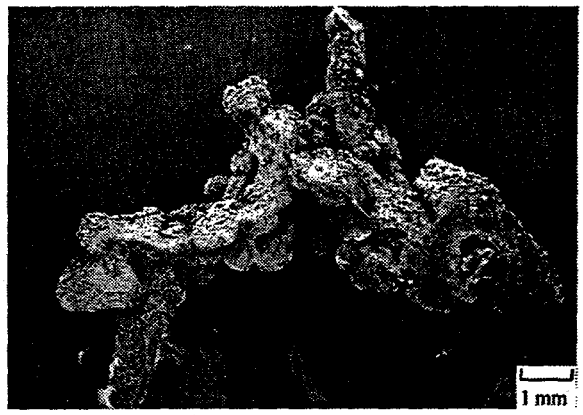

Fig. 7: Polycrystalline dendrite from Deposit 28 (10X).

This deposit was still very dendritic, however the dendrites did not slump, in contrast to the pure U deposits. The right cylindrical shape of the deposit is a result of shaping by deposit rotation past fixed scrapers. The mass of Deposit 30 was considerably higher than that of Deposit 3 (Fig. 2), 10.8 kg compared to 3.8 kg. The color of this and other U-Zr deposits was a dull gray; no shiny metallic features were visible.

The sample morphologies as viewed in the SEM were varied, but could generally be described as dendrite-shaped agglomerations of fine U grains, i.e. polycrystalline material. The more specific morphological types observed included leaf-like dendrite shapes, loose agglomerations of blocky fine crystals, aggregates of fine irregular grains, and also tangles of fine rhomboidal crystals similar to those observed in pure U deposits. No chains of large crystals were observed, however. Examples of typical morphologies are shown in Figs. 7 and 8, which show polycrystalline dendrites from Deposits 28 and 30. Close examination of the sample surfaces tended to reveal either blocky features reminiscent of intergranular fracture surfaces or fine-scale steps and ledges which appeared to be crystallographic in origin.

The concentration of Zr on the surfaces of the U-Zr deposit samples was semi-quantitatively evaluated using EDS. A wide variation of Zr concentrations, from approximately 6 to 100 wt.%, was found from sample to sample and also within single samples. There appeared to be no correlation of surface feature type or size with surface Zr concentration.

The internal structure of "typical" polycrystalline agglomerate dendrites reflected their external structure. Light microscopy examinations showed the dendrites to be polycrystalline; relatively fine grains were readily apparent on as-polished samples due to oxidation contrast. No extensive internal structure was observed, however porosity was still present, as shown in Fig. 9. The porosity tended to be slightly aligned along the long axes of the dendrites.

A second phase along the cross-section edges was observed for some of the U-Zr samples. This phase was bright (unoxidized, unlike the bulk U) in the light microscope and dark in the SEM (due to atomic number contrast). Fig. 10 is a closer view of Fig. 9 showing this phase. EDS analysis of the phase showed only a Zr peak, hence this phase was identified as α-phase Zr metal. The Zr phase was not observed in the interior of the cross-section, although occasionally a very thin, irregular line (approximately 0.5 µm thick) of the phase was found just to the interior of the cross-section edge. EDS analysis of the bulk, bright phase in the SEM showed only U peaks. No Zr was ever found in any form other than the dark phase, however it is possible that Zr could be present in quantities less than the detection limit of the EDS system used, approximately 0.5 wt.%.

The Zr phase was also found on the other morphological forms observed for the U-Zr deposits, most notably the rhomboidal crystals. The internal structure of these crystals was identical to that found for the pure U crystals—platelets oriented along the long axis of the crystal. On the surfaces of the crystals, however, a layer of Zr phase identical to that shown in Fig. 10 was present. No Zr phase was present on any of the internal surfaces.

A number of samples from Deposits 30 and 31 were taken at different locations in an attempt to observe systematic variations in sample morphology, surface Zr content, or presence of Zr phases with sample location. Inspection of Table 1 shows that there is no discernible trend present. Also, little correlation was found between the Zr surface concentrations, the presence of Zr phases in the cross-sections, and the overall morphologies. Some samples with more crystalline features, such as the Deposit 31 bottom outside sample, had larger quantities of Zr in evidence than other samples showing few or very fine features, such as the Deposit 31 top and middle outside samples.

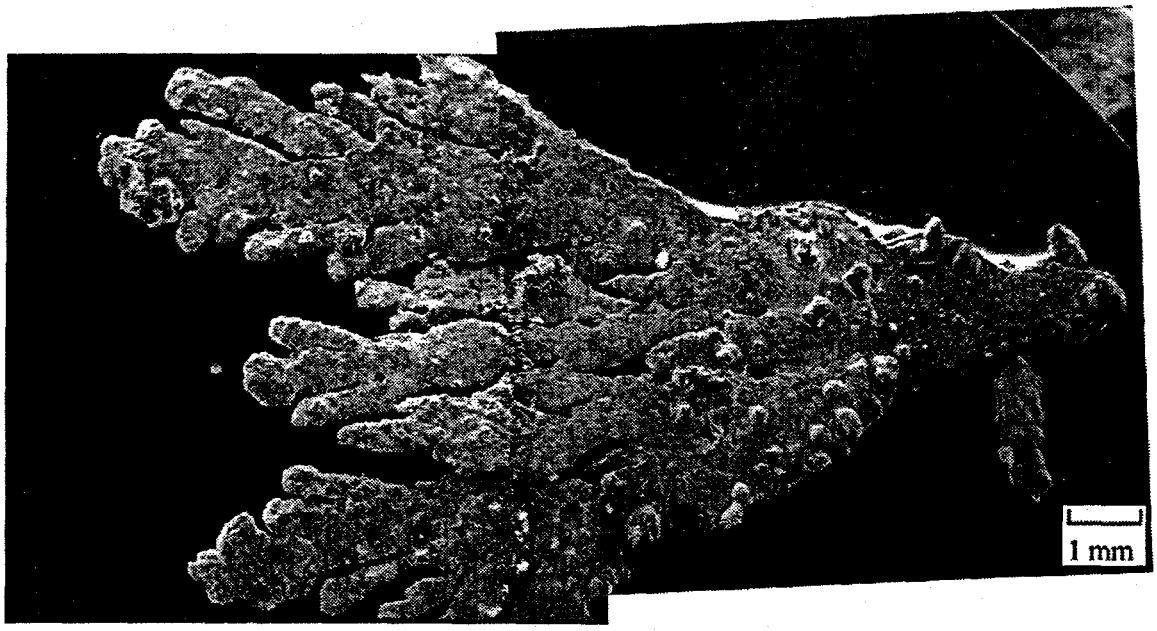

Fig. 8: Overview of a leaf-shaped dendrite from Deposit 30 (10X).

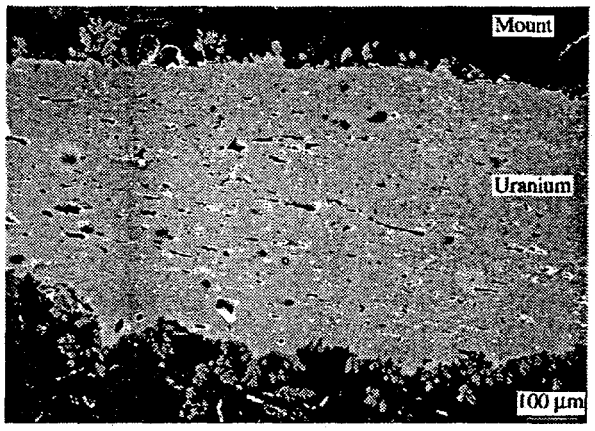

Fig. 9: Cross-section of a polycrystalline dendrite from Deposit 28 showing irregular porosity (1000X).

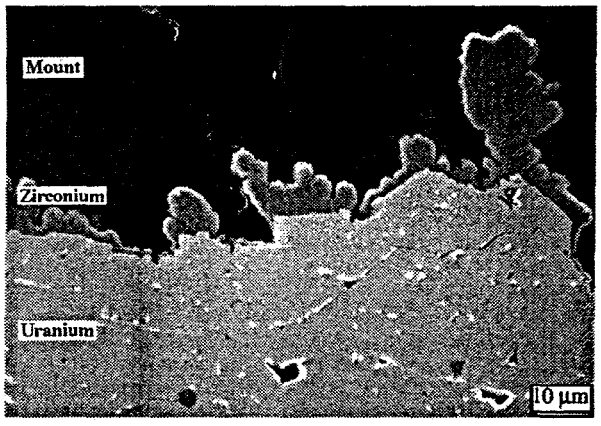

Fig. 10: Close-up of Fig. 8 showing Zr metal phase at the dendrite surface (1000X).

Discussion

Morphology of Pure U Deposits. The crystallographic, dendritic morphology of the pure U deposits is identical to that observed by previous researchers. Development of uranium electrorefining in molten chloride salts began in earnest in the late 1950's and 1960's by researchers at Argonne National Laboratory (5), the U.S. Bureau of Mines (7, 8), and in France (9, 10). Formation of dendrites composed of chains of linked rhomboidal crystals was always observed. Marzano and Noland (5) performed Laue X-ray diffraction on the crystals and determined that the preferred growth direction was (310). In fact, it appears to be very difficult to obtain U deposits which are not dendritic, as found by workers at Argonne trying to deposit uniform layers (11).

One aspect of the pure U crystal morphology which has not been previously reported is the complex internal structure of the crystals. A possible sequence for formation of the structure was presented above. Electrodeposition theory as it is currently understood does not provide an explanation for why individual dendrites would grow together to form apparently perfect larger crystals.

The Role of Zr in Electrodeposition. It is clear from the results presented in Section 3 that deposits containing quantities of Zr in excess of approximately 0.5 wt.% have morphologies which are significantly different from deposits containing no or very little Zr. The deposits which contain Zr in higher levels have a more fine-grained, polycrystalline character than pure U deposits, which are composed nearly exclusively of relatively large, rhomboidal crystals. In addition, the Zr-containing deposits show the presence of a second phase of pure Zr metal; this phase is observed only at or very near deposit surfaces. The morphology change appears to be linked to Zr presence in the deposit, and not just Zr presence in the electrorefining system. Deposit 25 (not discussed above) is a good example of a deposit for which Zr was present in the system but not in

the deposit. The average Zr content of the Deposit 25 dendrite samples, determined by analytical chemistry, was approximately 150 ppm. The morphology of the dendrites examined strongly resembled that of pure U deposits.

The obvious issue to be considered is the mechanism by which the presence of Zr in the deposit changes the growth morphology of uranium electrodeposition. The issue breaks down into two fundamental questions. First, why and how does Zr transport from the anode feed to the deposit, and second, how does the presence of Zr change the growth morphology?

Zr Oxidation and Deposition. A full discussion of Zr transport in the FCF electrorefiner is outside the scope of the present work, and the reader is referred to articles which discuss the chemical basis for electrorefining of spent nuclear fuel (12, 13). A simplified discussion is presented below.

In order for Zr to deposit at the cathode, it must exist in the salt (as $ZrCl_2$) in the immediate vicinity of the cathode surface. Since UCl_3 is more stable than $ZrCl_2$, any Zr^{2+} at the cathode will be preferentially reduced to the metal as compared to U^{3+}. At sufficiently high cell voltages, Zr^{2+} ions are produced in the salt by electrochemical oxidation of Zr metal at the anode. Zr metal is originally present as part of the U-10Zr alloy feedstock, and also can be present in the Cd pool incidental to the electrorefining process. Following oxidation, the Zr^{2+} ions are transported to the vicinity of the cathode, primarily via convection (stirring of the salt). Once they reach the cathode they will deposit.

The amount of Zr oxidized, expressed as a fraction of the total cell current, is predicted to vary over the course of an electrorefining run. The initial amount of Zr oxidized is low due to the difference in equilibrium cell potentials for Zr and U and the lower activity of Zr in the U-10Zr alloy compared to U. As the run progresses and U is oxidized from the alloy, the activity of Zr increases relative to the activity of U. This results in an increasing Zr oxidation current. Becauase the Zr deposition rate is dependent on the oxidation rate, a similar variance in Zr deposition rate will occur.

The observed location of Zr in the cross-sections of deposit samples, however, does not entirely fit with predictions of when Zr is deposited. The inconsistency is that Zr is only observed at or near the surfaces of deposits and not at all in the interior, contrary to the prediction of Zr deposition throughout the run. The statement that Zr is not observed in the interior must be predicated with knowledge of the detection limits of the EDS system which was used for microchemical analysis, which are on the order of 0.5 wt.%. Zr could therefore be present in undetectable impurity levels throughout the deposit.

Given that information, a few ways exist to reconcile prediction and observation. The first possibility is that Zr is present throughout the deposit as the analysis suggests—the concentrations might be undetectable in the centers of dendrites (the first material of the sample to deposit). If this were true, however, a gradation in Zr concentration through the thickness of the deposit corresponding to the variation in Zr current fraction may be expected to exist. Zr concentrations would be high (and therefore detectable) at the surface and gradually decrease until the limit of detection was reached. Such a concentration gradient was not observed; Zr was only found in discrete, pure Zr phases at the surface.

A second explanation, one more consistent with observations, is that Zr atoms are sufficiently mobile on the electrodeposited U surface to always be present at the surface and not be incorporated into the bulk metal. Two observations support this hypothesis. First, Zr has very limited solid solubility in α-phase U metal at the deposition temperature, less than 0.2 wt.% (14). Levels of Zr greater than the solubility limit would be rejected by the growing U lattice. Second, high diffusion coefficients can be achieved on the surfaces of growing electrodeposited metals due to a high vacancy concentration (15). Rapid solid state diffusion is the only requirement to maintain the "equilibrium" state of Zr and U—separation into two phases. This requirement is considered achievable at 773 K under conditions of high vacancy concentration on the dendrite surface and along the U-Zr interface. Phases with compositions corresponding to the UZr_2 intermetallic were not observed.

Zr Effects on Growth Processes. The question of how the presence of Zr atoms during the electrodeposition of U changes the morphology of the deposited U is difficult to answer using the experimental information available. The deposits examined were not created under carefully controlled conditions that might enable determination of the influences of specific variables, but rather as part of a large-scale process occurring remotely in a hot cell. The known fact is that deposits which contain significant quantities of Zr possess more polycrystalline attributes than pure U deposits. No other variable yet identified exerts such a strong influence on morphology.

Comparison of this fact with the available literature on electrodeposition suggests that Zr may be acting as an inhibitor in this system (16, 17). The action of an inhibitor is to promote denser and finer-grained deposits by occupying active surface sites on the growing lattice. An inhibitor can be any species which hinders the cathodic process present at the electrode surface, in the double layer, or in the diffusion zone. As an example, organic molecules are commonly used as inhibitors in electrodeposition from aqueous solutions to promote smooth deposits (16). The Zr^{2+} ion would be a strong candidate for an inhibitor because it is favorably reduced in comparison with uranium. It is therefore easily envisioned occupying active surface sites, forcing uranium atoms to nucleate new grains rather than continue to grow along preferred crystallographic planes.

The observed location of Zr in U-Zr deposits, especially viewed in relationship to the morphology of the sample, does not entirely support this hypothesis. Although deposits having Zr definitely appear more dense and tend to show more polycrystallinity, an example exists which appears to be in direct contradiction to this trend. The top outside sample from Deposit 28 was a short chain of large rhomboidal crystals which contained 3.5 wt.% Zr. The Zr was present as a 3-10 μm thick continuous layer on the outside surfaces of the crystals. If Zr acted as an inhibitor, any crystalline areas observed in U-Zr deposits would be expected to be associated with locally very low Zr concentrations, however it is also possible that the Zr layer was deposited at the end of the run after the U crystals had stopped growing (being fully formed), providing sort of an "overcoat". This example demonstrates that considerably more work is required to determine the deposition mechanisms operative in this system.

Performance Implications of Morphologies. The performance implications of the U-Zr deposit morphology in comparison with the pure U deposit morphology are fairly clear: better performance in terms of collection efficiency and total deposit weight is obtained for the U-Zr deposits. The total weights achieved for the pure U deposits were never greater than 8 kg; 10 kg weights were routinely obtained for U-Zr deposits. The collection

efficiencies for the pure U deposits examined varied from 9% to 25%, while the collection efficiencies for U-Zr deposits varied from 33% to 38%. These deposits were produced under a wide range of conditions, and no other variable shows as much effect on collection efficiency as does the presence or absence of Zr.

Such a performance improvement would be expected based on simple mechanical considerations of the two morphology types. The limits on deposit performance are set by the ability of the dendrites to withstand the process of shaping by rotation past the scrapers. As the outermost dendrites contact the scrapers, torsional shear forces are placed on the deposit which can lead to separation of dendrites either from themselves or the steel mandrel. Dendrites so separated fall into the Cd pool at the bottom of the electrorefiner, where they can be later recovered by using the Cd pool as an anode. Separation of dendrites results in lowered collection efficiency; indeed this is likely the main reason collection efficiencies closer to 100% are not obtained in the FCF electrorefiner. Very high collection efficiencies have been reported by previous researchers (5, 7, 8, 10, 18). The deposits collected in the previous studies were not rotated and subjected to stress in the form of scraper contact. The growing weight of the deposit itself will also provide stress to result in dendrite separation. The entire deposit mass, up to 11 kg, must be supported by the bond between the uranium deposit and the steel mandrel, and the dendrites must resist slumping under their own weight to avoid the bottom scraper.

Hence a few desirable mechanical properties are identified: (i) resistance to deformation of the dendrite chains, especially with respect to bending stresses; (ii) resistance to failure by separation; and (iii) good bonding between the deposit and the steel mandrel substrate (this may also be a chemical attribute). Comparison of the pure U and U-Zr deposit morphologies leads to the conclusion that the U-Zr deposits are expected to show better performance for the above measures. The dendrites for the pure U deposits tend to be composed of chains of single crystals. The resistance of the chains to bending and separation will be low because of the weak link between adjacent crystals (Fig. 4). Handling experience with samples of these deposits supports this conclusion; the chains are easily broken with tweezers by bending at the links. The more polycrystalline nature of the U-Zr deposits and more continuous nature of the dendrites suggests that they would have higher resistance to deformation, a position which is also supported by sample handling experience. The U-Zr samples tended to be much more difficult to pull apart. Due to the difficulty of obtaining suitable samples, a comparison of the deposit-substrate interface for the two types of deposits has not been performed, so no conclusions may be reached about the relative strengths of the deposit-mandrel bonds.

Conclusions

Examinations of pure U and U-Zr electrodeposits produced in the FCF electrorefiner at ANL-W were performed, and substantial differences were observed in the morphologies of the two types of deposits. Samples from pure U deposits were comprised of chains of U crystals with a characteristic rhomboidal shape and complex internal porosity structure. The morphologies of samples from deposits containing Zr in excess of approximately 0.5 wt.% showed more polycrystalline features. While some samples from U-Zr deposits still exhibited the crystalline morphology of the pure U deposits, most were comprised of polycrystalline dendrites or aggregates of fine grains. Zr was found to be present as a second, Zr metal phase at or very near the surfaces of the dendrites examined.

The implications of the observed morphologies were considered. The differences in morphologies of the pure U and U-Zr deposits suggest that Zr may be acting as an inhibitor for U electrodeposition, however the evidence supporting this hypothesis was not conclusive and in one instance was in apparent contradiction. The change in morphology due to Zr addition suggests that the better performance of the U-Zr deposits is likely a result of better mechanical properties of the U-Zr dendrites.

Acknowledgements

The author wishes to acknowledge the following people for assistance with this work: R.D. Mariani, E.L. Wood, K. Nissen, N. Bomono, R. Benedict, D.C. Crawford, and J.R. Krsul. This work was supported by the U.S. Department of Energy, Office of Nuclear Energy, Science and Technology, under contract W-31-109-Eng-38.

References

1 Goff, K.M., R.W. Benedict, and D. Levinskas, in Proc. Conf. on DOE Spent Nuclear Fuel – Challenges and Initiatives, Salt Lake City, UT, Dec. 1994, p. 282-87
2 Laidler, J.J., in Proc. Conf. on DOE Spent Nuclear Fuel – Challenges and Initiatives, Salt Lake City, UT, Dec. 1994, p. 188-95
3 Ackerman, J.P., T.R. Johnson, L.S.H. Chow, E.R. Carls, W.H. Hannum, and J.J. Laidler, Progress in Nuclear Energy 31, 141-154 (1997)
4 Goff, K.M., R.D. Mariani, D. Vaden, N.L. Bomono, and S.S. Cunningham, in Proc. Conf. on DOE Spent Nuclear Fuel and Fissile Material Management, Reno, NV, June 1996, p. 137-143
5 Marzano, C. and R.A. Noland, "The Electrolytic Refining of Uranium", Argonne National Laboratory Report ANL-5102 (1953)
6 Gay, E.C. and W.E. Miller, in Proc. Conf. on DOE Spent Nuclear Fuel – Challenges and Initiatives, Salt Lake City, UT, Dec. 1994, p. 267-274
7 Campbell, R.E. and T.A. Sullivan, "Electrorefining Uranium in a Chloride Electrolyte", U.S. Bureau of Mines Report 6624 (1964)
8 Cattoir, F.R. and T.A. Sullivan, "Molten-Salt Electrorefining of Uranium", U.S. Bureau of Mines Report 6507 (1964)
9 Boisde, G., G. Chauvin, H. Coriou, and J. Hure, Electrochimica Acta 5, 54-71 (1961)
10 Chauvin, G., H. Coriou, P. Jabot, and A. Laroche, J. Nucl. Mater. 11, 183-192 (1964)
11 Marshall, S.L., L. Redey, G.F. Vandegrift, and D.R. Vissers, "Electroformation of Uranium Hemispherical Shells", Argonne National Laboratory Report ANL-89/26 (1989)
12 Tomczuk, Z., J.P. Ackerman, R.D. Wolson, and W.E. Miller, J. Electrochem. Soc. 139, 3523-28 (1992)
13 Ackerman, J.P., Ind. Eng. Chem. Res. 29, 140 (1991)
14 Kassner, M.E. and D.E. Peterson, eds, "Phase Diagrams of Binary Actinide Alloys", ASM International, Materials Park, Ohio (1995)

15 Bockris, J.O.M. and A.K.N. Reddy, "Modern Electrochemistry", Vol. 2, Plenum Press, New York (1970)
16 Winand, R., Electrochimica Acta 39, 1091-1106 (1994)
17 Wranglen, G., Electrochimica Acta 2, 130-44 (1960)
18 Antill, J.E., D.S. Butler, and E. Barnes, p. 3, in "Progress in Nuclear Energy, Series V. Metallurgy and Fuels, H.M. Finneston and J.P. Howe eds., Permagon Press, New York (1959)